Materials Today Communications 25 (2020) 101603

Contents lists available at ScienceDirect

Materials Today Communications

journal homepage: www.elsevier.com/locate/mtcomm

Structure, electronic structure, optical and magnetic studies of double perovskite Gd_2MnFeO_6 nanoparticles: First principle and experimental studies

Ramesh Sivasamy [a,b,*], Potu Venugopal [c], Rodrigo Espinoza-González [a]

[a] Department of Chemical Engineering, Biotechnology and Materials, University of Chile, Beauchef 851, Santiago, 8370459, Chile
[b] Saveetha School of Engineering, Saveetha University, Chennai, Tamilnadu, 600077, India
[c] Department of Chemistry, Pondicherry University, Pondicherry 605014, India

ARTICLE INFO

Keywords:
Sol-gel synthesis
double perovskite
Rietveld refinement
First-Principle calculations
optical energy band-gap
magnetic properties

ABSTRACT

Multifunctional materials are greatly appealed in electrical, electronic and magnetic devices which are developed by several researchers for future device fabrications. Among such materials, the double perovskites with rare earth metals are actively studied. In this work, we synthesized the double perovskite Gd_2MnFeO_6 nanoparticles through a simple sol-gel process and studied the crystal structure, morphology, optical, electronic structure and magnetic characteristics. The orthorhombic crystal type with the *Pbnm* space group of the double perovskite Gd_2MnFeO_6 nanoparticles was confirmed using X-ray diffraction analysis. String-of-beads like a continuous network morphology were observed by scanning electron microscopy. The divergence in the spin-polarized electronic structures such as the density of states and band structure indicates the presence of magnetic properties in the compound. The nanoparticles show paramagnetic nature at room temperature and complex magnetic nature below room temperature.

1. Introduction

Single perovskites with the general formula ABO_3 (A = alkaline and rare-earths, B = transition metals) are identified as excellent materials for their interesting structural, optical, electrical and magnetic properties for multifunctional applications [1–3]. Despite the continuing dominance of single perovskites, it has recently found them to show insufficient performance and insufficient stability. In the meantime, the double perovskite structure can bring many significant advantages to the physicochemical properties, stability, and efficiency. Recently, the single perovskites were converted to double perovskites $AA'B_2O_6$ or $A_2BB'O_6$ (A = Rare-earths and alkaline earth, B = transition metals) by occupying the two different cations in the A or B sites [4]. These materials are constructed in the fashion of two single perovskites such as ABO_3 and $AB'O_3$ alternate to each other. The A-site cations behave as an electron donor to the BO_6 unit [5]. The double perovskites show an interesting structural, electronic, physical, and chemical properties [6]. Double perovskites may be the potential replacement of the conventional single perovskites for several reasons. First, they are expanding the compositional space of the perovskite family because they have more space to accommodate the new atoms [7]. Second, it creates complex atomic environments that can lead to electronic structures not commonly found in single perovskites. Third, it can show enhanced chemical stability under catalytic conditions, such as a wide range of oxidizing or reducing environments, acidic or basic solutions, and environments involving humidity, heat, light, or CO_2. The double perovskites are showing superior electrocatalysis, and photo (electro) catalysis, magnetocaloric, and thermoelectric performance. The mixture of rare-earth and transition metal double perovskites are turned to be significant materials because of their structural stability with controllable physical and chemical properties [7]. These significant properties mainly arise from the electronic interaction between 4f-3d rare-earth and transition metals. Amongst all the rare-earths, the gadolinium (Gd) is an interesting element because of its partially occupied 4f and 5d states which enables the inter (5d-5d) and intra (5d-4f) exchange interactions [8].

The structure, morphology and particle size of these double perovskites are definitely dependent on the dopants and synthetic techniques

* Corresponding author at: Nanoscale Functional Materials Laboratory, Department of Chemical Engineering, Biotechnology and Materials, Faculty of Physical Sciences and Mathematics, University of Chile, Piso 5, Office 533, 851-Beauchef, Santiago, Chile.
E-mail addresses: rsivasamy@ing.uchile.cl, rameshsiva_chem@yahoo.com (R. Sivasamy).

https://doi.org/10.1016/j.mtcomm.2020.101603
Received 26 February 2020; Received in revised form 7 August 2020; Accepted 23 August 2020
Available online 2 September 2020

In particular, the B site ordering double perovskites were reported as most fascinating for its physical properties that are strongly associated with the B-B interactions. These can be used in technological applications that comprise superconductivity, magnetic memory devices, sensors, optic devices, and magnetocaloric materials. In the reported $R_2MnB'O_6$ double perovskites, the Mn, Fe and rare-earth ions are making the compound structurally stable and magnetically interesting due to its complex magnetic ordering [9–11]. The magnetic exchange interactions between Mn^{4+}/Fe^{2+} ions facilitate the formation of ferromagnetic clusters, anti-ferromagnetic ordering, and the existence of spin-glass behavior. Currently, numerous synthetic techniques have been employed to synthesize the $R_2BB'O_6$ double perovskites, such as co-precipitation [12], solid-state reaction [13], hydrothermal [14], sol-gel [15], and decomposition techniques [16,17]. Among all these methods, the sol-gel technology is superior because of their easy controlled advantages, including the particle shape, structure, composition and product homogeneity.

As per the literature survey, there is no report available on the double perovskite of Gd_2MnFeO_6 nanoparticles. Hence, we focus on this work aimed to study the crystal structure, morphologies, electronic, optical absorbance and magnetic behavior of the double perovskite Gd_2MnFeO_6 nanoparticles prepared using a simple sol-gel method.

2. Experimental

2.1. Preparation of double perovskite Gd_2MnFeO_6 nanoparticles

Double perovskite Gd_2MnFeO_6 nanoparticles were prepared through the simple sol-gel process. Gadolinium acetate (Sigma-Aldrich, 99.9%), Iron acetate (Sigma-Aldrich, 99.9%), and manganese acetate (Himedia, 99.5%), and citric acid (Himedia, $C_6H_8O_7$; 99.7%) was used without further purification. Gadolinium, manganese and iron nitrates were prepared from the corresponding acetates and the nitrates were added separately to 2 M nitric acid (HNO_3) solution. All solutions (metal nitrates) were mixed together and stirred for about 2 h, Thereafter, 50 ml of 2 M citric acid solution was added. Then the pH (~7) of the whole solution mixture was altered using liquid ammonia to enhance the gel formation. The resulted solution was kept in stirring at 343 K until it transforms to gel. Then, it was dried at 373 K for 2 h to form a highly porous xerogel. Finally, it was sintered at 773 K for 6 h to get dense nanoparticles and cooled in the air. The schematic flowchart of the synthesis route is presented in Figure S1 (Supporting materials).

2.2. Characterizations

The phase purity and structural properties of the nanoparticles were obtained by an X'Pert PRO PANalytical X-ray diffractometer (XRD). The surface morphology and composition were examined using an TESCAN-VEGA3 electron microscope with energy dispersive X-ray analysis (SEM-EDX). The optical absorption spectrum was recorded using an UV-VIS diffuse reflectance spectrometer (Shimadzu 2600). The magnetic behavior was identified by an LAKESHORE VSM 7404 vibrating sample magnetometer (VSM) and quantum design; E2 PPMS (physical property measurement system).

2.3. Computational details

The geometry relaxation and electronic structure calculations were carried out by the density functional theory (DFT) using the Cambridge serial total energy package (CASTEP) code [18]. The generalized gradient approximation-Perdew-Burke-Ernzerhof (GGA-PBE) functional was implemented to obtain electronic structure calculations [19,20]. The convergence of geometry optimization was set On-the-fly generation (OTFG) norm-conserving pseudopotentials with Koelling-Harmon relativistic treatment. We used the Brillouin zone integration with 3 × 3x2 Monkhorst-Pack (MP) grid, and the cutoff energy was applied to 571 eV. The threshold conditions, such as maximum force, maximum displacement, maximum stress and maximum energy change, for the geometry convergence were set to 1.0×10^{-5}, 0.03 eV/ Å, 0.05 GPa and 0.001 Å.

3. Results and Discussion

3.1. X-ray diffraction

The phase identification, cell parameters, and average crystallite size of the Gd2 $MnFeO_6$ nanoparticles were revealed using room temperature powder XRD (PXRD) analysis. The PXRD pattern was indexed in the *Pbnm* space group. To get the structural information, the Rietveld refinement was executed with the use of FullProf package.

Subsequent refinements were carried out in the space group Pbnm employing the structural model of the assigned occupation sites are 4c for La, 4b for Mn/Fe whereas two oxygen atoms are located at 4c and 8d sites. The unit cell parameters (a = 5.5675, b = 5.5952, c = 7.8734) are related to the ideal orthorhombic perovskite. After sequential iterations good agreement between experimental and calculated patterns was achieved [22]. The refined cell parameters of a, b, c, unit cell volume (V) and calculated density (d) are equal to 5.6131, 7.5787 and 5.3259 Å, 226.56 $Å^3$, and 7.549 g/cm^3, correspondingly. The recorded and simulated XRD patterns are shown in Fig. 1. All the predominant peaks in the experimental pattern are well comparable with the simulated pattern. The refined crystal data and atomic positions were given in supporting materials (Tables T1-T3).

The Goldschmidt factor (t) is an essential factor to provide the structural information of the perovskites. In general, the tolerance factor for the cubic structure is 1 and for the tetragonal structure it is $1.00 > t > 0.97$. When tolerance factor is below 0.97, the octahedrons are distorted or tilted that leads to the lower symmetries like orthorhombic or monoclinic. The tolerance factor of the double perovskite ($A_2BB'O_6$) can be calculated by relation [21]

$$t = \frac{(rA) + rO}{\sqrt{2}\,(rB) + rO} \tag{1}$$

Where t denotes the tolerance factor rA, rO and rB are the ionic radii of ions A, B and O, respectively. In the orthorhombic structure of $A_2BB'O_6$ double perovskite, the Gd^{3+} ionic radius of 1.06 Å is appropriate for the A position, and Mn^{4+} (0.58 Å) and Fe^{2+} (0.64 Å) atoms are in the B and B' positions, respectively. The calculated tolerance factor of the double perovskite Gd_2MnFeO_6 nanoparticle is 0.905 which is in good relation with the orthorhombic structure of the compound.

The XRD pattern peak width is directly related to the crystallite size

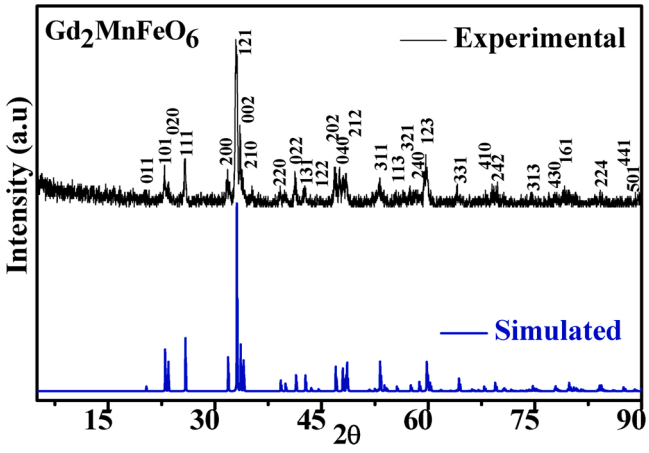

Fig. 1. Powder X-ray diffraction patterns of double perovskite Gd_2MnFeO_6 nanoparticles.

in the compound. The strong and broadened nature of the PXRD indicates the fnanocrystallite formation. The crystallite size was estimated by the Debye-Scherrer method with the use of equation 2 [22–24].

$$D = K\lambda/\beta\cos\theta \quad (2)$$

where D signifies the average crystallite size, K represents the Scherrer constant, λ stands for the CuKα radiation wavelength, β stands for the FWHM (full with of the half maximum) value and θ denotes the Bragg angle. The estimated average crystallite size of the nanoparticles was found to be 32 nm.

3.2. Structural information

The optimized double perovskite Gd2 MnFeO6 crystal structure and ion coordination are displayed in Fig. 2. The crystal structure consists of four formula units in which the oxygen atoms are occupied the Wyckoff positions 8*d* (O1; 1.2021, 0.5377, 0.72153) and 4*c* (O2; 1.0582, 0.7500, 1.0687), gadolinium ions are placed in 4*c* (Gd1; 0.5658, 0.2500, 1.0295) and the mixed manganese and iron ions occupied the position 4*a* (Mn/Fe; 0.000, 0.000, 0.000). In the crystal structure, six oxygen atoms are connected with the Mn/Fe ions (Mn/Fe-O_6) that form a complex octahedral geometry. The Mn/Fe-O_6 octahedron is distorted and that created three different bond lengths between Mn/Fe and O atoms (Mn/Fe-O1-2.0660, Mn/Fe-O1- 1.8893, Mn/Fe-O2-1.9571 A) in which one is along the b axis and the other two are along the c axis. Also, the bond angle has deviated from 180$\hat{0}$ to 150$\hat{0}$ and 155$\hat{5}$. The distraction in the bond lengths and bond angles is due to John-Teller effect.

3.3. Electronic structure

The DFT calculations were implemented to calculate the electronic structure of the double perovskite Gd_2MnFeO_6. The optimization energy (-21235.51 eV) reveals that the studied structure is stable and can be synthesized. The spin-polarized band structure and the partial density of states (PDOS) are shown in Figs. 3 and S2. The Fermi level is indicated in a stippled mark in the electronic structures. In the total band structure, the valence and conduction bands are passing through the Fermi region which indicates that the compound is metallic. To visualize further in detail, we implemented the spin-polarized electronic structure calculations, where the up spins are showing bandgap of 0.55 eV in the lower region of the Fermi level and the down spins are crossing the Fermi region in the band structure which indications that the studied compound is half-metallic. In partial DOS, the individual (Gd, Mn/Fe, and O1 and O2) electronic contributions are presented, in which the up spins and down spins are marked in up and down arrows. It is noticed that the down spin of the Gd 4f electrons is dominating at the conduction band minimum (CBM) and up spins of the Mn/Fe 3d electrons are dominating near the valence band maximum (VBM) in the energy region of -1 to 1 eV. The up and down spins of Gd 3d electrons are overlapping with the down spins of the Mn/Fe p-electrons. The Gd 4f up spin electrons are mainly contributing in -5 to −7 eV energy range. The Gd-4f and Mn/Fe-3d orbitals are overlapped by O-2p orbitals in the energy range between -5 and −10 eV. Also, the 2p electrons of O1 and O2 ions are significantly contributed to the VB region. From the band structure and density of states, the difference is observed between the up-spins and down-spins that confirms the half-metallic and ferromagnetic behavior of the studied compound.

3.4. Morphology analysis

The surface morphology, X-ray mapping and EDX quantitative measurement table of the Gd_2MnFeO_6 nanoparticles are presented in Fig. 4. From the SEM images, it is observed that the nanoparticles are fused to form the string-of-beads like continuous network structure such morphology was observed for different compounds synthesized by the solid-state reaction If the annealing time was long enough for the grain interdiffusion. Generally, such morphology indicates a homogeneous chemical composition and uniform phase composition [26–28]. The energy dispersive X-Ray analysis (EDX) confirms that only principal components of Gd, Fe, Mn, and O are present to expected composition ratios. From the X-ray mapping, it is observed that all the constituent elements are distributed homogeneously throughout the compound. The X-ray mapping and EDX-analysis reveal the purity of the nanoparticles which is in a good agreement with the results of X-ray diffraction analysis.

3.5. Spectroscopy studies (Ultraviolet-visible diffuse reflectance and Raman Spectroscopy)

The ultraviolet-visible diffuse reflectance spectroscopy (UV-Vis DRS) spectrum of the Gd_2MnFeO_6 nanoparticles was measured from 200 to 800 nm at 300 K, and it is presented in Fig. 5(a). The broad absorption band centered at 581 nm (2.1 eV) is due to the charge transfer between Mn(3d)-O(2p) electronic states. The optical energy band-gap was estimated by the Tauc plot (Fig. 5 (b)) with the use of equation 2 [25–27].

$$\alpha h\upsilon = A(h\upsilon - E_g)^n \quad (2)$$

where Eg is the band-gap, hυ represents the photon energy, α is the absorption coefficient, A is a constant and n denoted the transition type. The observed optical energy band-gap of the nanoparticle is 1.09 eV which is narrower than the band-gaps of other related reported (Gd_2NiMnO_6 =3.05 eV [30]; La_2MnNiO_6 = 1.5 eV [31]) nanoparticles.

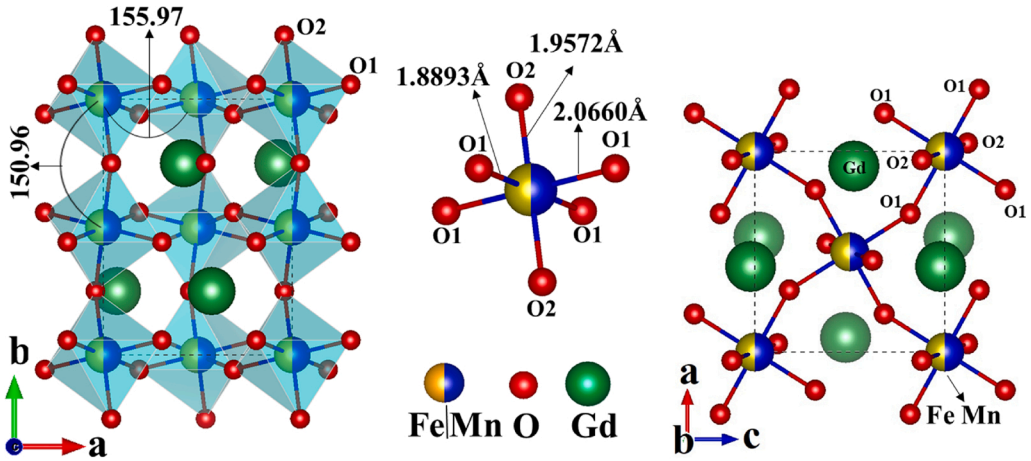

Fig. 2. Crystal structure and coordination environments of the crystallographic sites of double perovskite Gd_2MnFeO_6 nanoparticles.

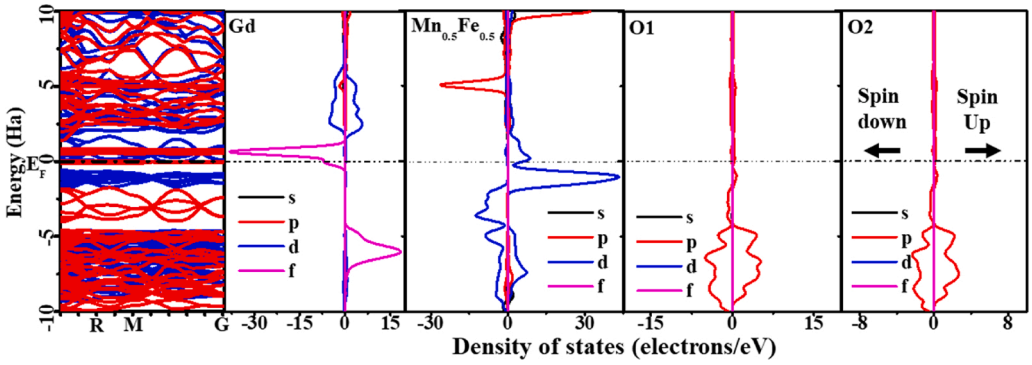

Fig. 3. Spin polarized band structures (Total, spin up, and spin down), and partial density of states of double perovskite Gd_2MnFeO_6 nanoparticles.

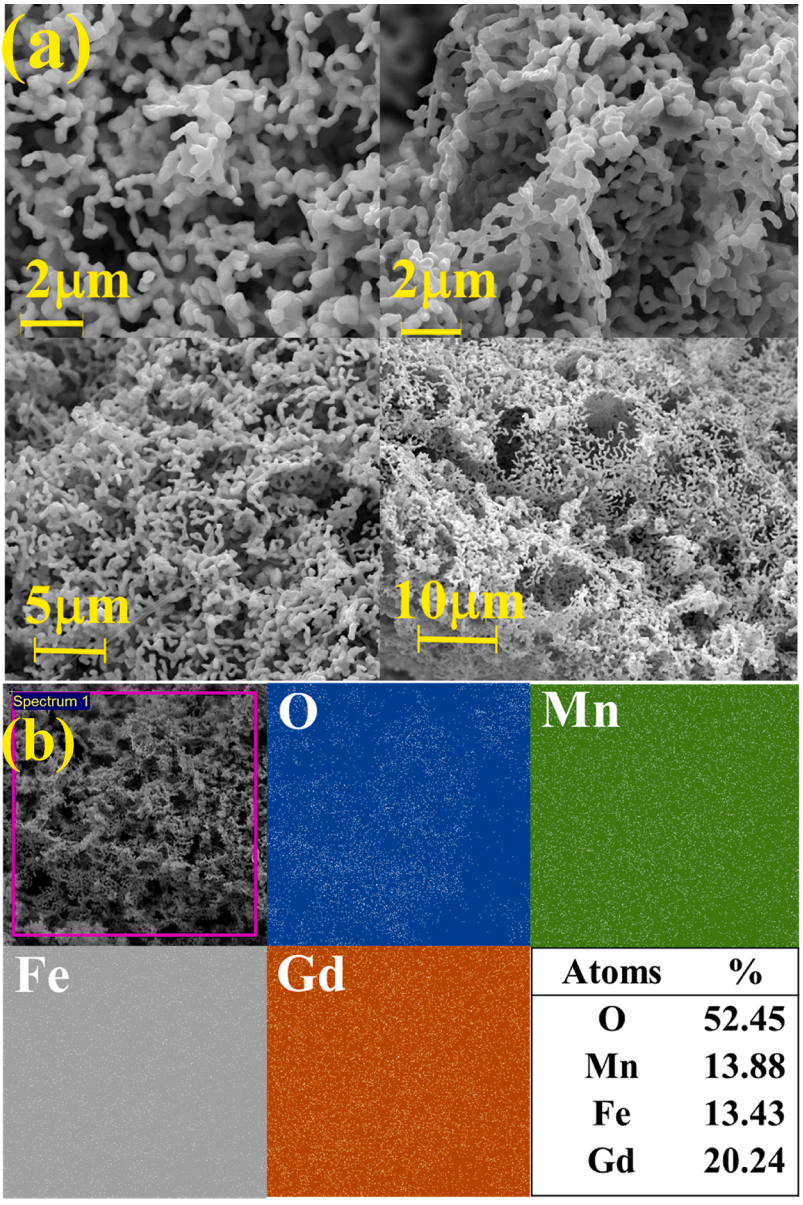

Fig. 4. (a) SEM images at different magnification, and (b) X-ray elemental mapping of double perovskite Gd_2MnFeO_6 nanoparticles.

The Fe/Mn ions integration into the lattice sites reduces the optical energy band-gap.

The Raman spectrum of the synthesized nanoparticles is shown in Fig. 5 (c). In general, the rare-earth orthorhombic manganites show 24 bands. The predominant peaks in Fig. 5 (c) were compared and assigned according to the earlier reported results [28]. The strong peak at

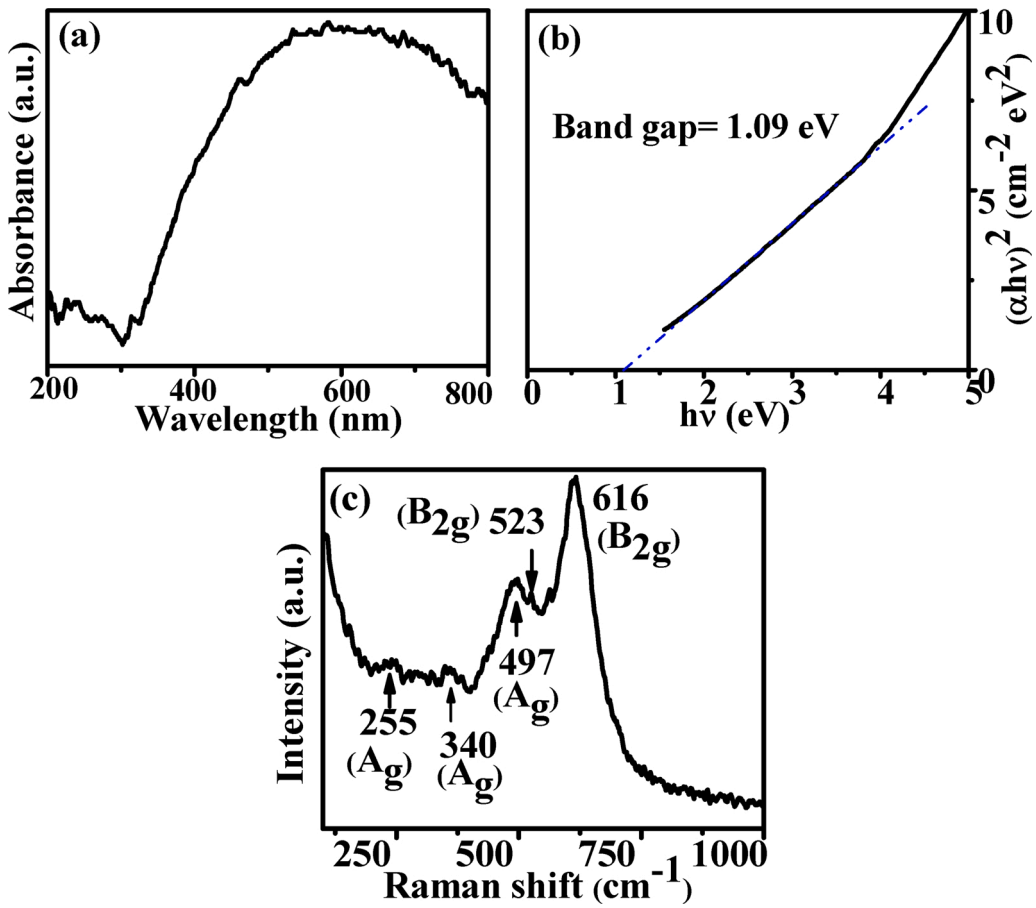

Fig. 5. (a) Optical absorption spectra, (b) optical band gap (Tauc plot) and (c) Raman spectra of double perovskite Gd_2MnFeO_6 nanoparticles.

616 cm^{-1} corresponds to the B_{2g} symmetric stretching mode. The shoulder peak at 523 cm^{-1} is attributed to B_2g symmetric rotational mode and the peat centered at 497 cm^{-1} appeared due to Ag symmetric starching mode. The peaks at 340 cm^{-1} and 255 cm^{-1} correspond to the Ag mode of distracted octahedral MnO_6 [29].

3.6. Magnetic Studies

The magnetization (Magnetic moment Vs Magnetic moment) curves with the applied magnetic field from -12,000 G to +12,000 G at different temperatures (320, 303, 120, 77, 38, 25 and 10 K) are presented in Figs. 6 (a) and S3. The hysteresis shape of the magnetization curves reveals the ferromagnetic behavior of the nanoparticles even at 320 K.

The magnetic characteristics such as magnetic susceptibility (χ), coercivity (Hc), remanence (Mr) and saturation (Ms) were obtained from the magnetization plots and the values are given in Table 1. The magnetic susceptibility (χ) was estimated by equation [32]:

$$M=\chi H \quad (3)$$

Where M represents the magnetization and H signifies the magnetic field. The field-dependent hysteresis curves are unsaturated even at the higher magnetic field (±12000 G). This unsaturation may be induced by the occurrence of the multi-domain ferromagnetic nanoparticles. The magnetic properties, such as magnetic Hc, Mr and Ms, are increased on

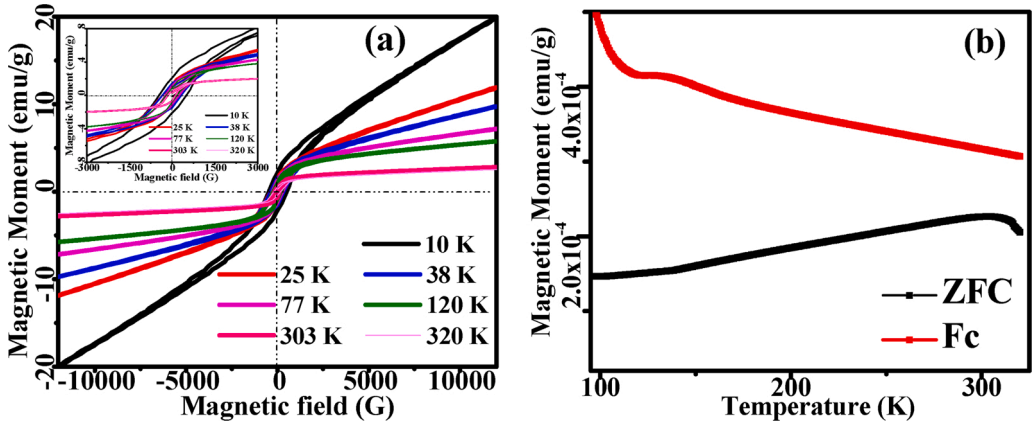

Fig. 6. (a) The magnetic hysteresis loop at various temperature, and (b) Induced magnetization curves (ZFC and FC) of double perovskite Gd_2MnFeO_6 nanoparticles.

Table 1
Magnetic Properties of double perovskite Gd_2MnFeO_6 nanoparticles.

Temperature (K)	Magnetic Properties			
	Susceptibility (χ)	Saturation (Ms) (emu/g)	Remanence (Mr) (emu/g)	Coercivity (Hc) (G)
320	6.1072×10^{-4}	2.5410	0.5672	108.52
303	2.2482×10^{-3}	2.8193	0.5841	121.23
120	1.3592×10^{-3}	5.7739	0.8379	197.17
77	1.0522×10^{-3}	7.2087	1.3178	241.61
38	2.6256×10^{-4}	9.7704	1.4323	308.26
25	1.7770×10^{-3}	11.8950	1.0140	324.92
10	4.4352×10^{-3}	19.9520	2.2331	508.22

temperature reducing from 300 to 10 K. The absence of sudden jerks in the hysteresis curves indicates that the compound has good mechanical stability due to low residual strain and high homogeneity.

To further investigate the magnetic behavior of the synthesized nanoparticles, the field cooled and zero-field cooled (FC, and ZFC) magnetic curves were obtained from 320 to 100 K by applying the external magnetic field of 1.2 T, as displayed in Fig. 6 (b). In Fig. 6 (b), it is seen that, on decreasing the temperature, the FC curve maintains almost a steady trend whereas the ZFC curves show decreasing against magnetization. The divergence between the FC and ZFC curves reveals ferromagnetic nature even at 320 K. In general, the gadolinium-based manganese oxide systems show multiple exchange interactions such as ferromagnetic double interchange interaction (Mn^{4+}-O-Mn^{3+}) and antiferromagnetic super-interchange interaction (Gd^{3+}-O-Gd^{3+} and Mn^{3+}-O-Mn^{3+},) and negative exchange interactions between 3d(Fe^{2+}/Mn^{4+})-O2-4f (Gd^{3+}) electrons [20]. Also, the deviation of Fe/Mn^{3+}-O-Fe/Mn^{4+} angle from the 180̊ leads to a decrease in ferromagnetic nature, not the antiferromagnetic nature. However, in the present compound, the large ferromagnetic Fe dopant and dominating the double exchange interactions (Fe/Mn^{3+}-O-Fe/Mn^{4+}) confirms the ferromagnetic nature of the compound.

4. Conclusions

In summary, the multifunctional orthorhombic double perovskite Gd_2MnFeO_6 nanoparticles were synthesized by the simple sol-gel process. The calculated optical energy band-gap was found to be 1.09 eV. The ferromagnetic behavior was confirmed by temperature dependence magnetization plots, ZFC and FC. The estimated narrow optical energy band-gap and magnetic properties of the double perovskite Gd_2MnFeO_6 nanoparticles can offer this material as magnetically separable catalyst.

Data availability

The raw/processed data required to reproduce these findings cannot be shared at this time due to technical or time limitations.

Declaration of Competing Interest

The authors declared no competing interests in this paper.

CRediT authorship contribution statement

Ramesh Sivasamy: Conceptualization, Methodology, Formal analysis, Writing - review & editing. **Potu Venugopal:** Methodology, Data curation, Visualization, Writing - original draft. **Rodrigo Espinoza-González:** Supervision, Validation.

Declaration of Competing Interest

The authors report no declarations of interest.

Acknowledgements

The author Ramesh Sivasamy expressing his thanks to the FONDECYT for Project-N°
3170052.

Appendix A. Supplementary data

Supplementary material related to this article can be found, in the online version, at doi:https://doi.org/10.1016/j.mtcomm.2020.101603.

References

[1] R. Sivasamy, P. Venugopal, R. Espinoza-Gonzalez, Crystal structure, optical and magnetic properties of perovskite $Gd(Mn_{0.7}Ni_{0.3})O_3$ ceramic nanoparticles: an experimental and first-principles studies, Ceram. Int. 45 (2019) 20022–20027.
[2] P.P. Ma, X.M. Chen, Further ordering structural investigation of $Ba((Co,Zn,Mg)_{1/3}Nb_{2/3})O_3$ perovskites by Raman spectroscopy, Mater. Charact. 158 (2019), 109938.
[3] X. Er, Y. Zhang, Y. Yin, C. Wang, H. Wang, J. Zhang, Q. Zhan, Atomic structure of domain and defect in layered-perovskite Bi_2WO_6 thin films, Mater. Charact. 154 (2019) 395–399.
[4] S.M. Borchani, W.C.-R. Koubaa, M. Megdiche, Structural, magnetic and electrical properties of a new double-perovskite $LaNaMnMoO_6$ material, Roy. Soc. Open Sci. 4 (2017), 170920.
[5] H. Chen, A. Millis, Design of new Mott multiferroics via complete charge transfer: promising candidates for bulk photovoltaics, Sci. Rep. 7 (2017) 6142.
[6] I.N. Bhatti, I.N. Bhatti, R.N. Mahato, M.A.H. Ahsan, Physical properties in nano-crystalline Ho_2CoMnO_6, Ceram. Int. 46 (2020) 46–55.
[7] J.L. Rosas, J.M. Cervantes, J. León-Flores, E. Carvajal, J.A. Arenas, M. Romero, R. Escamilla, DFT study on the electronic and magnetic properties of the Sr_2FeNbO_6 compound, Mater. Today Commun. 23 (2020), 100844.
[8] B.B. Das, S. Ramesh, Synthesis, structural and magnetic characterization of $Ag_{3(2+x)}Gd_xTi_{4-x}O_{11+\delta}$ ($0 \leqslant x \leqslant 1.0$) nanocomposites, AIP Conf. Proc. 85 (2008) 1003.
[9] R.X. Silva, R.M. Almeida, R.L. Moreira, R. Paniago, M.V.S. Rezende, C.W. A. Paschoal, Vibrational properties and infrared dielectric features of Gd_2CoMnO_6 and Y_2CoMnO_6 double perovskites, Ceram. Int. 45 (2019) 4756–4762.
[10] Y. Jia, X. Zhang, Z. Zhang, L. Li, Effect of sintering temperature on microstructure and magnetic properties of double perovskite Y_2CoMnO_6, Ceram. Int. 44 (2018) 19794–19799.
[11] Y. Zhang, H. Li, G. Dan, L. Hou, X. Li, Z. Ren, G. Wilde, Cryogenic magnetic properties and magnetocaloric performance in double perovskite Pr_2NiMnO_6 and Pr_2CoMnO_6 compounds, Ceram. Int. 44 (2018) 20762–20767.
[12] M. Penchal Reddy, X.B. Zhou, L. Jing, Q. Huang, Microwave sintering, characterization and magnetic properties of double perovskite La_2CoMnO_6 nanoparticles, Mater. Lett. 132 (2014) 55–58.
[13] A.T. Fulmer, J. Dondlinger, M.A. Langell, Passivation of the La_2NiMnO_6 double perovskite to hydroxylation by excess nickel, and the fate of the hydroxylated surface upon heating, Appl. Surf. Sci. 305 (2014) 544–553.
[14] G. Zhang, G. Li, F. Liao, Y. Fu, M. Xiong, J. Lin, Crystal growth and magnetic properties of the double perovskites R_2MnNiO_6 (R=Pr, Sm and Ho) by a hydrothermal route, J. Cryst. Growth 327 (2011) 262–266.
[15] F.N. Mansoorie, J. Singh, A. Kumar, Wet chemical synthesis and electrochemical performance of novel double perovskite Y_2CuMnO_6 nanocrystallites, Mater. Sci. Semicond. Process. 107 (2020), 104826.
[16] A. Hossain, A.K.M. Atique Ullah, P. Sarathi Guin, S. Roy, An overview of La_2NiMnO_6 double perovskites: synthesis, structure, properties, and applications, J. Sol-Gel Sci. Technol. 93 (2020) 479.
[17] B. Mercey, P.A. Salvador, W. Prellier, T.-D. Doan, J. Wolfman, M. Hervieu, B. Raveau, Thin film deposition: a novel synthetic route to new materials, J. Mater. Chem. 9 (1999) 233–242.
[18] S. Ramesh, S. Marutheeswaran, J.V. Ramaclus, D.C. Paul, Electronic structure study on 2D hydrogenated Icosagens nitride nanosheets, Superlatt. Microstruct. 76 (2014) 213–220.
[19] G. Kaliyan, R. Sivasamy, R. Espinoza-Gonzalez, Electronic structure, optical and thermodynamic studies on 2D $SnSe_2$ nanosheet: a first-principles investigation, Superlatt. Microstruct. 133 (2019), 106182.
[20] S. Ramesh, P. Venugopal, E. Mosquera, Experimental and theoretical investigation of Bixbyite $(Mn_{0.8}Ni_{0.2})_2O_3$ nanoparticles for magnetic and electrochemical applications, J. Magn. Magn. Mater. 443 (2017) 45–50.
[21] C.J. Bartel, C. Sutton, B.R. Goldsmith, R. Ouyang, C.B. Musgrave, L.M. Ghiringhelli, M. Scheffler, New tolerance factor to predict the stability of perovskite oxides and halides, Sci. Adv. 5 (2019) eaav0693.
[22] R. S, J.V. Ramaclus, B.B. Das, E. Mosquera, Structural, morphological, optical and magnetic properties of $Ag_{3(2+x)}In_xNb_{4-x}O_{11+\delta}$ ($0.25 \leq x \leq 1.0$) nanoparticles synthesized by sol–gel method, Mater. Res. Bull. 105 (2018) 121–125.
[23] S. Ramesh, B.B. Das, Synthesis, structure and characterization of $Nd_{2X}Cd_{2-3X}SiO_4$ ($0.01 \leq X \leq 0.21$) solid-solutions, J. Kor. Chem. Soc. 55 (2011) 502–508.
[24] R. Sivasamy, P. Venugopal, E. Mosquera, Synthesis of Gd_2O_3/CdO composite by sol-gel method: structural, morphological, optical, electrochemical and magnetic studies, Vacuum 175 (2020) 109255.

[25] S. Ramesh, J.V. Ramaclus, E. Mosquera, B.B. Das, Sol–gel synthesis, structural, optical and magnetic characterization of $Ag_{3(2+x)}Pr_xNb_{4-x}O_{11+\delta}$ ($0.0 \leq x \leq 1.0$) nanoparticles, RSC Adv. 6 (2016) 6336–6341.
[26] A. Barde, D.P. Joubert, Investigation of structural, mechanical, dynamic, electronic and optical properties of seleno-germanates A_2GeSe_4 (A = Mg, Ca and γ-Sr) from first principles, Mater. Today Commun. 22 (2020), 100785.
[27] R. Sivasamy, P. Venugopal, K.V. Kumar, R. Espinoza-González, Synthesis and characterizations of $Pd/Mn(Mn_{1.36}Pd_{0.64})O_4$ nanocomposite: an experimental and theoretical approach, Vacuum 182 (2020) 109683.
[28] J. Laverdière, S. Jandl, A.A. Mukhin, V.Y. Ivanov, V.G. Ivanov, M.N. Iliev, Spin-phonon coupling in orthorhombic $RMnO_3$ (R= Pr, Nd, Sm, Eu, Gd, Tb, Dy, Ho, Y: A Raman study, Phys. Rev. B 73 (2006), 214301.
[29] J. Oliveira, J. Agostinho Moreira, A. Almeida, V.H. Rodrigues, M.M.R. Costa, P. B. Tavares, P. Bouvier, M. Guennou, J. Kreisel, Structural and insulator-to-metal phase transition at 50 GPa in $GdMnO_3$, Phys. Rev. B 85 (2012), 052101.
[30] R. Mohassel, A. Sobhani, M.S. Niasari, Investigation of photocatalytic, electrochemical, optical and magnetic behaviors of rare-earth double perovskites using combustion synthesized Gd_2NiMnO_6 nanostructures in the presence of different saccharides, Int. J. Hydrogen Energy 44 (2019) 860.
[31] Aslam Hossain, A.K.M. Atique Ullah, Partha Sarathi Guin and Sanjay Roy, An overview of La_2NiMnO_6 double perovskites: synthesis, structure, properties, and applications, J. Sol-Gel Sci. Technol. 93 (2020) 479.
[32] S. Ramesh, Sol-gel synthesis and characterization of $Ag_{3(2+x)}Al_xTi_{4-x}O_{11+\delta}$ ($0.0 \leq x \leq 1.0$) nanoparticles, J. Nanosci. 2013 (2013) 1–9.